Chapter 1
Computational Aspects of Maximum Likelihood DOA Estimation of Two Targets with Applications to Automotive Radar

Philipp Heidenreich and Abdelhak M. Zoubir

Abstract Direction-of-arrival (DOA) estimation of two targets with a single snapshot plays an important role in many practically relevant scenarios in automotive radar for driver assistance systems. Conventional Fourier-based methods cannot resolve closely spaced targets, and high-resolution methods are required. Thus, we consider the maximum likelihood DOA estimator, which is applicable with a single snapshot. To reduce the computational burden, we propose a grid search procedure with a simplified objective function. The required projection operators are pre-calculated off-line and stored. To save storage space, we further propose a rotational shift of the field of view such that the relevant angular sector, which has to be evaluated, is centered with respect to the broadside. The final estimates are obtained using a quadratic interpolation. An example is presented to demonstrate the proposed method. Also, results obtained with experimental data from a typical application in automotive radar are shown.

Keywords Automotive radar • Direction of arrival (DOA) • Driver assistance systems • Maximum likelihood (ML) estimation

P. Heidenreich (✉)
ADC Automotive Distance Control Systems GmbH, Peter-Dornier-Str. 10, 88131 Lindau, Germany
e-mail: philipp.heidenreich@continental-corporation.com

A.M. Zoubir
Signal Processing Group, Technische Universität Darmstadt, Merckstr. 25, 64283 Darmstadt, Germany
e-mail: zoubir@spg.tu-darmstadt.de

G. Schmidt et al. (eds.), *Smart Mobile In-Vehicle Systems: Next Generation Advancements*, DOI 10.1007/978-1-4614-9120-0_1,

1.1 Introduction

Ever-increasing amount of advanced signal processing algorithms is used in various automotive applications [1, 2], e.g., advanced driver assistance systems [3]. These utilize from various sensors to determine the environment of a vehicle. From an identified traffic situation, the driver assistance system regulates the behavior of the vehicle, instructs the driver, or warns the driver in dangerous situations. Often radar sensors are employed, which work reliably even in bad weather conditions, and can provide accurate measurements of the range and relative velocity of multiple targets. To also measure the lateral position of a target, an array of antennas in horizontal direction with digital beamforming can be applied. For typical applications such as collision avoidance or adaptive cruise control (ACC), it is essential to accurately estimate the lateral position and to be able to resolve multiple closely spaced targets. For the array system with limited aperture, this can be achieved with high-resolution processing, which is considered computationally intensive and numerically complex, so that real-time implementation becomes a challenging task.

A pulsed radar system with an array of receive antennas can be effectively used for target localization in terms of range, relative velocity, and direction of arrival (DOA) [4, 5]. After radar preprocessing, which consists of a pulse compression and a Fourier transform over the pulses, the received sensor data is divided into processing cells according to the range and relative velocity, each represented by a single snapshot. For more details, an exemplary radar system is described in [6].

In most practical situations of automotive radar, multiple targets can be distinguished by their range and/or relative velocity so that each processing cell contains at most one target. In the single-target case, the optimal DOA estimates can be found using the Beamformer (BF) spectrum, which is computationally simple [7]. However, there are situations in which multiple targets have similar range and relative velocity so that they are superposed in a processing cell. We consider the situation with two targets per processing cell as practically relevant. In the ACC application, this is motivated by experimental data and may occur when there is an horizontal multipath with a close guardrail, as depicted in Fig. 1.1. If the two propagation paths fall into the same processing cell and cannot be resolved, this generally results in a false localization of the observed car, which seems to be pulled towards the guardrail. To correctly localize the observed car and a ghost target, high-resolution DOA estimation is required. Note that the multipath situation can be correctly identified using the guardrail location, which can be estimated from stationary target detections.

A number of high-resolution DOA estimators are available in the literature, see, e.g., [7–9]. Among the subspace methods, there is the popular MUSIC algorithm [10], which requires an eigendecomposition of the spatial covariance matrix, and a one-dimensional search on a fine grid to obtain the DOA estimates. For particular array geometries, there are also analytic solutions, e.g., unitary ESPRIT [11]. Implementing an eigendecomposition on a practical system with real-time constraints can be numerically complex. Eigendecomposition is iterative in nature

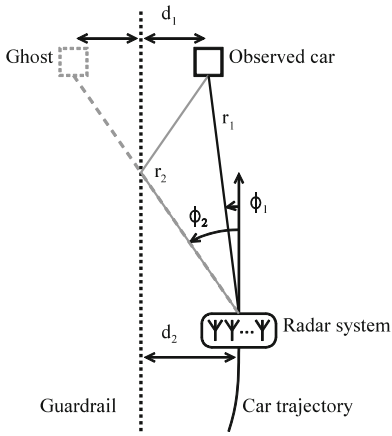

Fig. 1.1 Automotive radar situation with horizontal multipath with a close guardrail

and therefore hard to parallelize [12]. Moreover, when only a single snapshot is available, decorrelation techniques are required so that the signal subspace is fully represented. This can be achieved using the forward/backward (FB) averaging and/or spatial smoothing [13], which is suboptimal in general and can result in a reduction of the array aperture. The described drawbacks can limit the practical usage of subspace methods.

In contrast, the maximum likelihood (ML) DOA estimator of multiple targets can be directly applied with a single snapshot. It is asymptotically efficient [14] and possesses an improved threshold performance when compared to subspace methods [15]. Further, it allows resolving correlated targets [8]. Despite its good properties, the ML estimator has not enjoyed much practical application due to its high computational cost. It requires the optimization of a multidimensional objective function with a complicated multi-model shape. Computationally efficient but iterative implementations are the method of alternating projections [16] or the relaxation algorithm (RELAX) in [17].

Here, for the two-target case, we consider a global search of the two-dimensional ML objective function as practically feasible. We propose to use a simplified calculation of the objective function and a delimited search range. The required projection operators are data independent and can be pre-calculated off-line, which enables a trade-off between the computational complexity and the required storage space.

1.2 Signal Model

Let $\boldsymbol{x}$ denote the M-element array vector, or snapshot, from a pre-detected processing cell according to the range and relative velocity, whose power is significantly above the noise level. The problem formulation is posed as follows: decide between the single-target model and the two-target model

$$\begin{aligned} D = 1: &\quad \boldsymbol{x} = s_0 \boldsymbol{a}(\psi_0) + \boldsymbol{n} \\ D = 2: &\quad \boldsymbol{x} = s_1 \boldsymbol{a}(\psi_1) + s_2 \boldsymbol{a}(\psi_2) + \boldsymbol{n} \end{aligned} \tag{1.1}$$

and estimate the respective parameters. s_0 and ψ_0 are the target response parameter and DOA parameter in the single-target model, respectively. Likewise, s_1, s_2, ψ_1, and ψ_2 are the corresponding parameters in the two-target model.

$$\boldsymbol{a}(\psi) = \frac{1}{\sqrt{M}} \left[1, e^{j\psi}, \ldots, e^{j(M-1)\psi}\right]^T \tag{1.2}$$

but the steering vector of the considered uniform linear array (ULA) with electrical angle $\psi = \frac{2\pi}{\lambda} d \sin\phi$, where λ is the wavelength, d is the array element spacing, and ϕ is the spatial azimuth angle. The measurement noise vector $\boldsymbol{n}$ is assumed to be spatially white, circular complex Gaussian with zero mean and variance σ^2.

1.3 Optimal Processing

The optimal processing is described in the following. It consists of the ML DOA estimation for the single-target model and the two-target model and a generalized likelihood ratio test (GLRT).

1.3.1 Maximum Likelihood for One Target

The ML estimator for ψ_0 in model (1.1) for $D = 1$ corresponds to the location of the global maximum of the BF spectrum:

$$P(\psi) = \left|\boldsymbol{a}(\psi)^H \boldsymbol{x}\right|^2.$$

The inner vector product corresponds to a spatial Fourier transform at frequency ψ. Hence, $P(\psi)$ can be evaluated efficiently using a Fast Fourier transform (FFT) with zero-padding.

Let the step size of the evaluation grid be $\Delta\psi$, and let the location of the global maximum on the evaluation grid be ψ_n. A refined DOA estimate can be obtained using a quadratic interpolation in the neighborhood of ψ_n as

$$\hat{\psi}_0 = \psi_n + 0.5\Delta\psi \frac{P(\psi_{n-1}) - P\left(\psi_{n+1}\right)}{P(\psi_{n-1}) - 2P(\psi_n) + P\left(\psi_{n+1}\right)}$$

1.3.2 Maximum Likelihood for Two Targets

The ML estimators for ψ_1 and ψ_2 in model (1.1) for $D = 2$ correspond to the location of the global maximum of the two-dimensional ML objective function:

$$c(\psi_1, \psi_2) = \boldsymbol{x}^H \boldsymbol{P}_{\boldsymbol{A}}(\psi_1, \psi_2)\boldsymbol{x} \tag{1.3}$$

where

$$\boldsymbol{P}_{\boldsymbol{A}}(\psi_1, \psi_2) = \boldsymbol{A}\left(\boldsymbol{A}^H\boldsymbol{A}\right)^{-1}\boldsymbol{A}^H, \quad \boldsymbol{A} = [\boldsymbol{a}(\psi_1), \boldsymbol{a}(\psi_2)]$$

is the projection matrix onto the column span of steering matrix $\boldsymbol{A}$. An intuitive interpretation is that we seek for parameters ψ_1 and ψ_2 which maximize the projection of $\boldsymbol{x}$ onto the plane spanned by the columns of $\boldsymbol{A}$.

The optimization of $c(\psi_1,\psi_2)$ needs to be numerical and is generally computationally intensive. Below, we describe the direct calculation of the objective function and a global search procedure.

1.3.2.1 Direct Objective Function Evaluation

To determine projection matrix $\boldsymbol{P}_{\boldsymbol{A}}(\psi_1,\psi_2)$, the matrix inverse of $\boldsymbol{A}^H\boldsymbol{A}$ is required. Using the inversion formula for a matrix of dimension two, and notation $\boldsymbol{a}_1 = \boldsymbol{a}(\psi_1)$ and $\boldsymbol{a}_2 = \boldsymbol{a}(\psi_2)$ for convenience, we have

$$\boldsymbol{P}_{\boldsymbol{A}}(\psi_1, \psi_2) = \frac{1}{1 - |\beta|^2}\left(\boldsymbol{a}_1\boldsymbol{a}_2^H - \beta\boldsymbol{a}_1\boldsymbol{a}_2^H - \beta^*\boldsymbol{a}_2\boldsymbol{a}_1^H + \boldsymbol{a}_2\boldsymbol{a}_2^H\right)$$

where $\beta = \boldsymbol{a}_1^H\boldsymbol{a}_2$, and we have used $\boldsymbol{a}(\psi)^H\boldsymbol{a}(\psi) = 1$. This allow us to calculate directly (1.3) using

$$c(\psi_1, \psi_2) = \frac{1}{1 - |\beta|^2}\left(|y_1|^2 - 2\mathrm{Re}\{\beta y_1^* y_2\} + |y_2|^2\right) \tag{1.4}$$

where $y_1 = \boldsymbol{a}_1^H\boldsymbol{x}$ and $y_2 = \boldsymbol{a}_2^H\boldsymbol{x}$. Provided all steering vectors are available on a discrete grid of the field of view, a significant part of the computational cost, required to evaluate a single point of (1.4), constitutes the calculation of y_1, y_2, and β, which corresponds to $12M$ real-valued multiply–add operations.

1.3.2.2 Global Search

Due to the complicated multimodal shape of the objective function $c(\psi_1,\psi_2)$, a numerical search procedure, e.g., using a damped Newton method, critically

depends on the initialization [18]. A fairly reliable initialization without eigendecomposition appears difficult to find, especially when the targets are not resolved in the BF spectrum. Here, we consider a global evaluation of the two-dimensional objective function on a selected grid for ψ_1 and ψ_2. Unlike numerical search procedures, this allows a non-iterative implementation.

Let $\psi_{1,m}$ and $\psi_{2,n}$ be the location of the global maximum on the evaluation grid with step size $\Delta\psi$; refined DOA estimates can be obtained using a quadratic interpolation in the neighborhood of the global maximum, as

$$\hat{\psi}_1 = \psi_{1,m} + 0.5\Delta\psi \frac{c(\psi_{1,m-1}, \psi_{2,n}) - c(\psi_{1,m+1}, \psi_{2,n})}{c(\psi_{1,m-1}, \psi_{2,n}) - 2c(\psi_{1,m}, \psi_{2,n}) + c(\psi_{1,m+1}, \psi_{2,n})}$$

$$\hat{\psi}_2 = \psi_{2,n} + 0.5\Delta\psi \frac{c(\psi_{1,m}, \psi_{2,n-1}) - c(\psi_{1,m}, \psi_{2,n+1})}{c(\psi_{1,m}, \psi_{2,n-1}) - 2c(\psi_{1,m}, \psi_{2,n}) + c(\psi_{1,m}, \psi_{2,n+1})}$$

Regarding computational cost, the global evaluation of the objective function is required only for $\psi_1 < \psi_2$. Note that the resulting triangular search range is shown in Fig. 1.2 (top right). The corresponding computational cost is

$$C = C_1 N_2, \quad N_2 = \frac{N_\psi (N_\psi - 1)}{2}$$

where C_1 represents the computational cost, required to evaluate a single point of the objective function; N_2 is the number of points in the two-dimensional search range; and N_ψ is the number of grid points in the field of view, $\psi \in [-\pi, \pi)$.

1.3.3 Generalized Likelihood Ratio Test

According to the model (1.1) for $D = 1$ and $D = 2$, let the unknown parameters be collected in vectors $\boldsymbol{\Theta}_1$ and $\boldsymbol{\Theta}_2$, respectively, and let $p_1(\boldsymbol{x}|\boldsymbol{\Theta}_1)$ and $p_2(\boldsymbol{x}|\boldsymbol{\Theta}_2)$ be the corresponding likelihood functions, i.e., the conditional probability density function of the snapshot given the unknown parameter. A GLRT for deciding between the single-target model and the two-target model is

$$T = \frac{\max_{\boldsymbol{\Theta}_2} p_2(\boldsymbol{x}|\boldsymbol{\Theta}_2)}{\max_{\boldsymbol{\Theta}_1} p_1(\boldsymbol{x}|\boldsymbol{\Theta}_1)} > \gamma$$

which involves the determination of the corresponding ML estimates. For the signal model in Sect. 1.2, and taking the logarithm, the GLRT can be simplified to [19]

$$\log T = M \log \hat{\sigma}_1^2 - M \log \hat{\sigma}_2^2 > \log \gamma$$

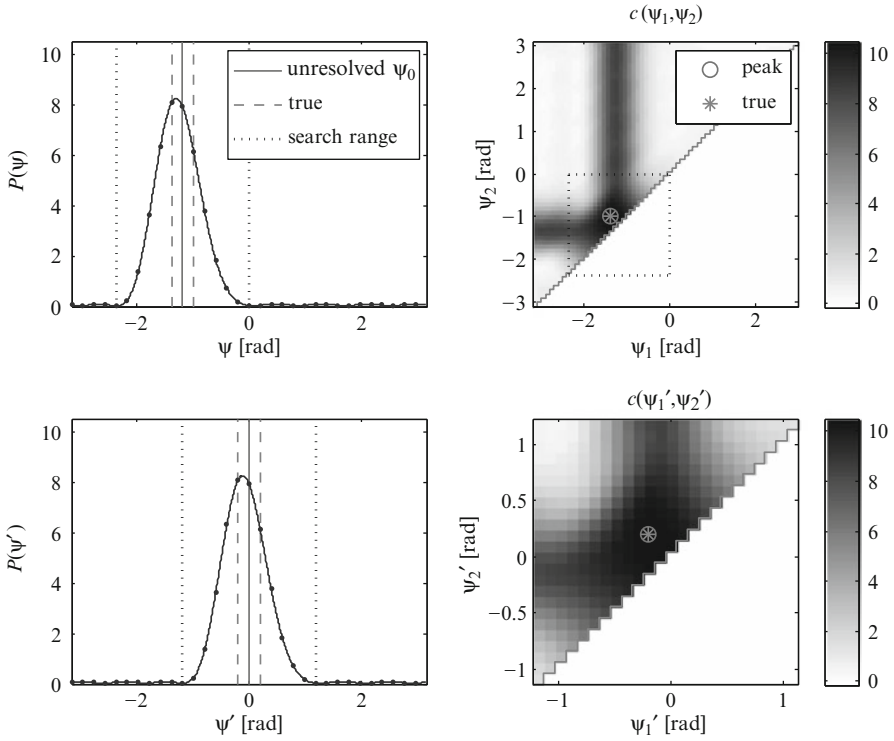

Fig. 1.2 Example with $M = 8$, two targets separated by $\psi_2 - \psi_1 = 0.5$BW, noise-free and single snapshot: BF spectrum to identify relevant angular sector (*top left*), ML objective function for full search range with $\Delta\psi = \pi/32$ (*top right*), shifted BF spectrum (*bottom left*), and ML objective function for shifted delimited search range (*bottom right*)

where

$$\hat{\sigma}_1^2 = \frac{1}{M}\left\|\boldsymbol{x} - \boldsymbol{a}(\hat{\psi}_0)\boldsymbol{a}(\hat{\psi}_0)^H\boldsymbol{x}\right\|^2, \quad \hat{\sigma}_2^2 = \frac{1}{M}\left\|\boldsymbol{x} - \boldsymbol{P}_{\boldsymbol{A}}(\hat{\psi}_1, \hat{\psi}_2)\boldsymbol{x}\right\|^2$$

A suitable threshold value $\log \gamma$ can be determined numerically, according to the Neyman–Pearson principle.

1.4 Proposed Approach

If multiple snapshots of the same processing cell, say at different cycles n, are considered, model (1.1) extends to $\boldsymbol{x}[n]$, $n = 1, \ldots, N$, where N is the number of available snapshots. In this case, the ML objective function in (1.3) extends to

$$c(\psi_1, \psi_2) = \frac{1}{N} \sum_{n=1}^{N} \boldsymbol{x}[n]^H \boldsymbol{P}_{\boldsymbol{A}}(\psi_1, \psi_2) \boldsymbol{x}[n] = \mathrm{Tr}\left\{ \boldsymbol{P}_{\boldsymbol{A}}(\psi_1, \psi_2) \hat{\boldsymbol{R}} \right\} \tag{1.5}$$

where

$$\hat{\boldsymbol{R}} = \frac{1}{N} \sum_{n=1}^{N} \boldsymbol{x}[n] \boldsymbol{x}[n]^H$$

is the sample covariance matrix. We remark that the single-snapshot case is of primary importance for the considered application. However, to enhance the DOA estimation accuracy, it may be desirable to combine multiple snapshots, which have been associated on a tracking procedure. Therefore, we consider the general case with N snapshots and comment on the special case with $N = 1$.

Note that in the case of multiple snapshots, one has to trade off between the evaluation of the quadratic term and the trace notation in (1.5).

1.4.1 Simplified Objective Function Calculation

The projection operator $\boldsymbol{P}_{\boldsymbol{A}}(\psi_1, \psi_2)$ is data independent; therefore, it can be pre-calculated off-line and stored. In this case, the calculation of the trace notation in (1.5) requires $C_1 = 4M^2$ real-valued multiply–add operations (note that only the diagonal entries of the matrix product have to be evaluated). Moreover, this can be simplified since $\boldsymbol{P}_{\boldsymbol{A}}(\psi_1, \psi_2)$ has a great deal of structure to exploit. In particular, it is centro-Hermitian, i.e., we have

$$\boldsymbol{J}_M \boldsymbol{P}_{\boldsymbol{A}}(\psi_1, \psi_2)^* \boldsymbol{J}_M = \boldsymbol{P}_{\boldsymbol{A}}(\psi_1, \psi_2)$$

where $\boldsymbol{J}_M$ is the exchange matrix of size M, with ones on the anti-diagonal and zeros elsewhere. This property can be easily shown [19] and directly follows from the fact that the steering vector, defined in (1.2), is Hermitian symmetric up to a complex scaling.

As a consequence, the ML objective function remains unchanged when snapshot $\boldsymbol{x}$ is replaced by $\boldsymbol{J}_M \boldsymbol{x}^*$, since

$$(\boldsymbol{J}_M \boldsymbol{x}^*)^H \boldsymbol{P}_{\boldsymbol{A}}(\psi_1, \psi_2) \boldsymbol{J}_M \boldsymbol{x}^* = \left[\boldsymbol{x}^H \boldsymbol{J}_M \boldsymbol{P}_{\boldsymbol{A}}(\psi_1, \psi_2)^* \boldsymbol{J}_M \boldsymbol{x} \right]^* = \boldsymbol{x}^H \boldsymbol{P}_{\boldsymbol{A}}(\psi_1, \psi_2) \boldsymbol{x}$$

where we have used the fact that $c(\psi_1, \psi_2)$ is real-valued by definition. Likewise, it remains unchanged when $\hat{\boldsymbol{R}}$ is replaced by the forward/backward (FB) averaged sample covariance matrix

$$\hat{\boldsymbol{R}}_{\mathrm{FB}} = \frac{1}{2}\left(\hat{\boldsymbol{R}} + \boldsymbol{J}_M \hat{\boldsymbol{R}}^* \boldsymbol{J}_M\right)$$

which is centro-Hermitian by definition.

1.4.1.1 Unitary Transformation

Let $\boldsymbol{Q}_M$ be a column conjugate symmetric matrix, satisfying $\boldsymbol{J}_M \boldsymbol{Q}_M^* = \boldsymbol{Q}_M$. A sparse choice for a unitary column conjugate symmetric matrix is

$$\boldsymbol{Q}_{2m+1} = \frac{1}{\sqrt{2}} \begin{bmatrix} \boldsymbol{I}_m & \boldsymbol{0} & j\boldsymbol{I}_m \\ \boldsymbol{0}^T & \sqrt{2} & \boldsymbol{0}^T \\ \boldsymbol{J}_m & \boldsymbol{0} & -j\boldsymbol{J}_m \end{bmatrix}$$

where $\boldsymbol{I}_m$ is the identity matrix of size m. An equivalent unitary column conjugate symmetric matrix of dimension $2m$ can be obtained by deleting the center row and center column of $\boldsymbol{Q}_{2m+1}$. The main result of [20] is that any square centro-Hermitian matrix is equivalently expressed by a real-valued matrix of the same dimension so that

$$\boldsymbol{V}(\psi_1, \psi_2) = \boldsymbol{Q}_M^H \boldsymbol{P}_A(\psi_1, \psi_2) \boldsymbol{Q}_M \tag{1.6}$$

and

$$\hat{\boldsymbol{C}} = \boldsymbol{Q}_M^H \hat{\boldsymbol{R}}_{\mathrm{FB}} \boldsymbol{Q}_M \tag{1.7}$$

are the real-valued projection operator and the sample covariance. The similarity transformation with unitary matrix $\boldsymbol{Q}_M$ is referred to as unitary transformation. We note that this approach has been used in [11] and [21], respectively, to derive the unitary ESPRIT and unitary root-MUSIC algorithm, where computational cost is reduced by replacing a complex-valued eigendecomposition by a real-valued one. Since we got $\boldsymbol{Q}_M \boldsymbol{Q}_M^H = \boldsymbol{I}_M$, the objective function in (1.5) can be rewritten as

$$\begin{aligned} c(\psi_1, \psi_2) &= \mathrm{Tr}\left\{ \boldsymbol{P}_A(\psi_1, \psi_2) \hat{\boldsymbol{R}} \right\} \\ &= \mathrm{Tr}\left\{ \boldsymbol{P}_A(\psi_1, \psi_2) \boldsymbol{Q}_M \boldsymbol{Q}_M^H \hat{\boldsymbol{R}}_{\mathrm{FB}} \boldsymbol{Q}_M \boldsymbol{Q}_M^H \right\} \\ &= \mathrm{Tr}\left\{ \boldsymbol{Q}_M^H \boldsymbol{P}_A(\psi_1, \psi_2) \boldsymbol{Q}_M \boldsymbol{Q}_M^H \hat{\boldsymbol{R}}_{\mathrm{FB}} \boldsymbol{Q}_M \right\} \\ &= \mathrm{Tr}\left\{ \mathbf{V}(\psi_1, \psi_2) \hat{\boldsymbol{C}} \right\}. \end{aligned} \tag{1.8}$$

To further reduce computational cost, we exploit that $\mathbf{V}(\psi_1,\psi_2)$ and $\hat{\boldsymbol{C}}$ are symmetric and remove redundant matrix entries [19]. In this case, and provided

Table 1.1 Computations required for evaluating a single point of the objective function, C_1, and storage space, in the single-snapshot case, using $N_2 = N_\psi(N_\psi - 1)/2$

	C_1	Storage space
Direct (1.4)	$\approx 12M$	$N_\psi 2M$
Simplified (1.8)	$(M + 1)M/2$	$N_2(M + 1)M/2$
Simplified (1.9)	$\approx 4M$	$N_2 2M$

all projection operators are available on a discrete grid of the two-dimensional search range, the calculation of (1.8) requires $C_1 = (M + 1)M/2$ real-valued multiply–add operations.

1.4.1.2 Single-Snapshot Alternative

In the single-snapshot case, an alternative is to employ an eigendecomposition of the real-valued projection operator in (1.6),

$$\boldsymbol{V}(\psi_1, \psi_2) = \boldsymbol{v}_1 \boldsymbol{v}_1^T + \boldsymbol{v}_2 \boldsymbol{v}_2^T$$

where eigenvectors $\boldsymbol{v}_1, \boldsymbol{v}_2 \in \mathbb{R}^{M \times 1}$ are both functions of ψ_1 and ψ_2. Again, the projection operator eigenvectors can be pre-calculated off-line and stored. Using $\boldsymbol{y} = \boldsymbol{Q}_M^H \boldsymbol{x} \in \mathbb{C}^{M \times 1}$, the objective function in (1.3) can be rewritten as

$$c(\psi_1, \psi_2) = \boldsymbol{y}^H \boldsymbol{V}(\psi_1, \psi_2) \boldsymbol{y} = \boldsymbol{y}^H \left(\boldsymbol{v}_1 \boldsymbol{v}_1^T + \boldsymbol{v}_2 \boldsymbol{v}_2^T \right) \boldsymbol{y} = |z_1|^2 + |z_2|^2 \tag{1.9}$$

where $z_1 = \boldsymbol{v}_1^T \boldsymbol{y}$ and $z_2 = \boldsymbol{v}_2^T \boldsymbol{y}$. Provided all projection operator eigenvectors are available on a discrete grid of the two-dimensional search range, a significant part of (1.9) constitutes the calculation of z_1 and z_2, which corresponds to $C_1 \approx 4M$ real-valued multiply–add operations.

1.4.1.3 Comparison

The overall cost of a global search has been described in Sect. 1.3.2.2. A trade-off between the computations, required for evaluating a single point of the objective function C_1 (in real-valued multiply–add operations), and the required storage space (in real-valued numbers) is given in Table 1.1 for the single-snapshot case. Note that the calculation of the real-valued projection operators, or respective eigenvectors, is done off-line and does not contribute to the overall cost. Also, the preprocessing, such as the formation of the covariance matrix, has no significant effect, as it is performed only once.

For an eight-element ULA and for the single-snapshot case, the simplified objective function in (1.9) is the cheapest option, both in terms of required

computations and the storage space. However, when multiple snapshots are available, we prefer the simplified objective function in (1.8), because the covariance matrix is employed and no extensions are necessary.

Regarding the storage, the simplified calculation requires the real-valued projection operators, or respective eigenvectors, on a two-dimensional search range with N_2 points, whereas the direct calculation only requires the steering vectors on a one-dimensional grid of the field of view.

1.4.2 Delimited Search Range

So far, we have reduced the computational cost by simplifying the calculation of the ML objective function. Next, we consider a delimited search range so that the number of points to evaluate on a two-dimensional search range and the storage space is reduced.

We only consider the more difficult case of closely spaced targets, which cannot be reliably resolved in the BF spectrum, i.e., $\psi_2 - \psi_1 < \mathrm{BW}$, where $\mathrm{BW} = 2\pi/M$ is the Rayleigh beamwidth. We remark that when the targets are widely separated so that they are reliably resolved in the BF spectrum, there exist computationally simple methods to reduce the estimation bias due to the leakage effect [22].

Let $\hat{\psi}_0 \in [\psi_1, \psi_2]$ be the peak location of the unresolved targets in the BF spectrum. Consider the shifted array output model, which is obtained by a rotational shift of the field of view:

$$\boldsymbol{x}' = \sqrt{M}\boldsymbol{a}(-\hat{\psi}_0) \odot \boldsymbol{x} = s_1 \boldsymbol{a}\left(\psi_1'\right) + s_2 \boldsymbol{a}\left(\psi_2'\right) + \boldsymbol{n}' \tag{1.10}$$

where $\psi_1' = \psi_1 - \hat{\psi}_0$ and $\psi_2' = \psi_2 - \hat{\psi}_0$ are the shifted DOA parameters and $\odot$ is the element-wise Hadamard product. The random characteristics of the rotationally shifted noise vector $\boldsymbol{n}'$ remain unchanged. The rotational shift allows to evaluate $c(\psi_1', \psi_2')$ on a delimited search range, e.g., $\psi' \in [-1.5\mathrm{BW}, 1.5\mathrm{BW}]$, which very likely contains the centered DOA parameters ψ_1' and ψ_2'. As a result, the number of points in the two-dimensional search range, N_2, and therewith the storage space of the projection operators have been reduced significantly. For the given example, the reduction corresponds roughly to $(3\mathrm{BW}/2\pi)^2 = (3/M)^2$.

1.4.3 Example

We present an example to demonstrate the principle of the delimited search range and the rotational shift. A ULA with $M = 8$ elements, spaced by $d = \lambda/2$, is used. A noise-free single snapshot is simulated according to model (1.1) for $D = 2$, with

target response parameters $s_1 = \sqrt{2}e^{-j\pi/4}s_2 = 1$, and an angular separation of $\psi_2 - \psi_1 = 0.5\text{BW}$. Figure 1.2 shows the results.

The upper and lower left plots show the BF spectra of the original snapshot and the shifted snapshot, respectively. Since the targets are not resolved in the BF spectrum, the unresolved peak ψ_0 can be used to identify the relevant sector for the delimited search range, which is indicated by the dotted lines. The upper and lower right plots show the ML objective function with step size $\Delta\psi = \pi/32$ for the full search range and the shifted delimited search range, respectively, which correspond to $\psi \in [-\pi, \pi)$ and $\psi' \in [-1.5\text{BW}, 1.5\text{BW}]$.

1.5 Experimental Data Analysis

We present results obtained with experimental data from a typical application in automotive radar. The scenario with horizontal multipath and a close guardrail, as shown in Fig. 1.1, is considered again. The two propagation paths, corresponding to the observed car and the ghost target, fall into the same processing cell if $r_2 - r_1 < \Delta r$, where Δr is the size of a range cell. The range and DOA parameters are related by

$$\begin{aligned} r_1 \sin(\phi_1) &= d_2 - d_1 \\ r_2 \sin(\phi_2) &= d_2 + d_1 \end{aligned}$$

where d_1 and d_2 are the normal distances from the guardrail.

The employed radar system operates at carrier frequency 24 GHz and has a range resolution of 1.8 m. For DOA estimation, an array of microstrip patch antennas in the form of a ULA with $M = 7$ elements, spaced by $d = \lambda/2$, is used. In the selected recording, the car with the radar system is following another car on the left lane of the motorway. In roughly 300 cycles, the distance of the observed car increases from 25 to 50 m.

For extracting relevant processing cells an initial DOA is determined by the peak of the BF spectrum. Relevant processing cells are extracted as follows:

- Detection, to select only cells with significant energy
- Clustering of cells with neighboring range, similar relative velocity, and initial DOA
- Gating, to consider only cells of interest for a certain application, whose relative velocity and initial DOA fall into a desired gate

The proposed ML estimator for two targets from Sect. 1.4 and the GLRT from Sect. 1.3.3 are applied to all relevant processing cells. For two selected cycles, Fig. 1.3 shows the camera recording of the scene and the result of the radar target localization as a function of x- and y-position.

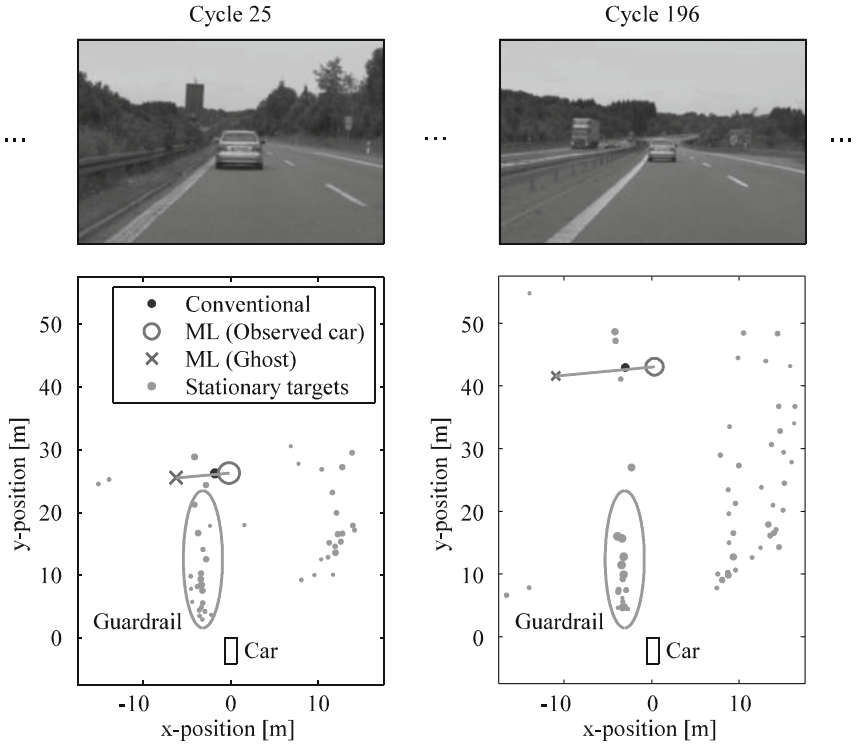

Fig. 1.3 Experimental data analysis. Scenario and all detected and clustered targets in bird's eye view for two selected cycles

Gray dots correspond to stationary targets, while black dots correspond to moving targets in the relevant gate, both for single-target DOA estimates. The result of the proposed ML estimator for two targets is indicated with a circle and cross, corresponding to the observed car and ghost target, respectively. On average, the measured power of the ghost target is roughly 6 dB smaller than the power of the observed car. The marker size of all displayed targets is proportional to the measured SNR. Note that the indicated stationary target detections can be used to localize the guardrail, which is required to identify the multipath situation.

Figure 1.4 shows the DOA estimation results of all cycles versus range. Note that the two selected cycles from Fig. 1.3 are indicated. In the upper plot, we show the conventional results with single-target DOA estimation using the BF. In the lower plot, however, we display improved results from two-target ML DOA estimation.

It can be observed from Fig. 1.4 that for the selected situation the conventional single-target DOA estimates tend to erroneously localize the observed car closer to the guardrail. When the multipath propagation is identified correctly, it is possible to apply the proposed ML estimator for two targets and adequately localize the observed car and a ghost target.

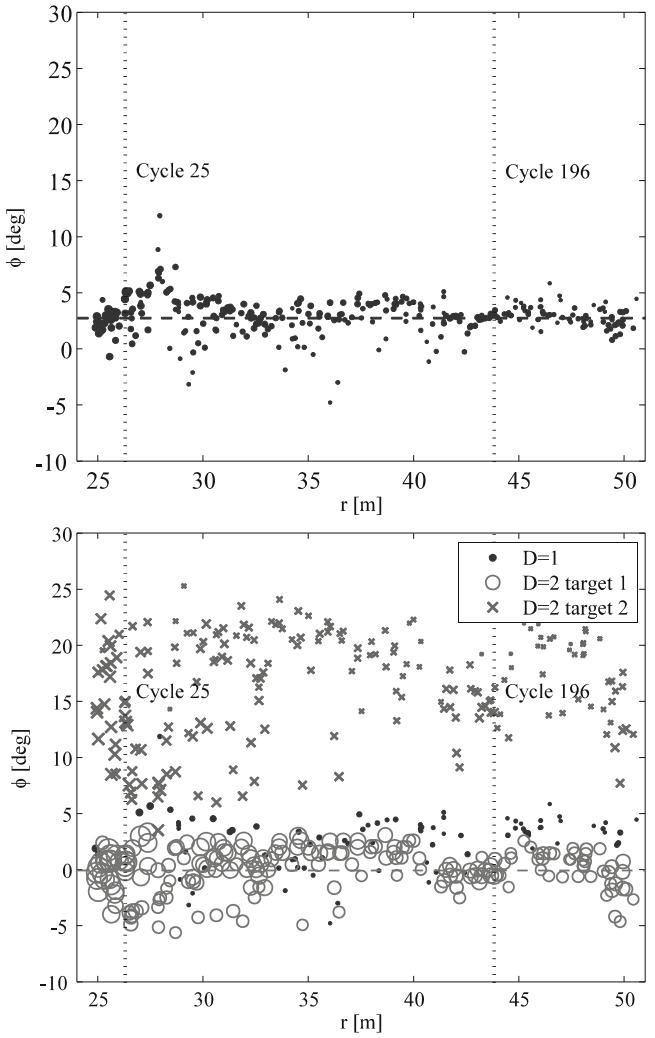

Fig. 1.4 Experimental data analysis. DOA estimates versus range: conventional results with single-target DOA estimation using the BF (*top*), improved results with two-target ML DOA estimation (*bottom*)

1.6 Conclusions

We have considered the practically relevant problem of high-resolution DOA estimation and detection of up to two targets. We have proposed a fast implementation of a grid search ML estimator, in which the ML objective function has been simplified and the required projection operators are pre-calculated off-line and stored. For saving storage space and computations, we have proposed a rotational

shift of the field of view such that the relevant angular sector, which has to be evaluated, is delimited and centered with respect to the broadside. The proposed method allows a computationally simple and straightforward implementation. The principle of the proposed method has been demonstrated using an example with simulated data. Finally, we have presented results obtained with experimental data from a typical application in automotive radar, in which high-resolution DOA estimation results in enhanced target localization.

References

1. J. Hansen, P. Boyraz, K. Takeda, H. Abut, *Digital Signal Processing for In-Vehicle Systems and Safety* (Springer, New York, 2011)
2. F. Gustaffson, Automotive safety systems. IEEE Signal Process. Mag. **26**(4), 32–47 (2009)
3. H. Winner, S. Hakuli, G. Wolf, *Advanced Driver Assistance Systems Handbook* (Vieweg + Teubner, Wiesbaden, 2009) (in German: Handbuch Fahrerassistenzsysteme: Grundlagen, Komponenten und Systeme für aktive Sicherheit und Komfort)
4. M. Skolnik, *Radar Handbook* (McGraw-Hill, New York, 2008)
5. M. Richards, *Fundamentals of Radar Signal Processing* (McGraw-Hill, New York, 2005)
6. M. Wintermantel, Radar system with improved angle formation, Germany Patent Application WO 2010/000252, 2010
7. H. Krim, M. Viberg, Two decades of array signal processing research. IEEE Signal Process. Mag. **13**(4), 67–94 (1996)
8. H. van Trees, *Detection, Estimation, and Modulation Theory—Part IV Optimum Array Processing* (Wiley, New York, 2002)
9. E. Tuncer, B. Friedlander, *Classical and Modern Direction-of-Arrival Estimation* (Academic Press, New York, 2009)
10. R. Schmidt, Multiple emitter location and signal parameter estimation. IEEE Trans. Antennas Propag. **34**(3), 276–280 (1986)
11. M. Haardt, J. Nossek, Unitary ESPRIT: how to obtain increased estimation accuracy with a reduced computational burden. IEEE Trans. Signal Process. **43**(5), 1232–1242 (1995)
12. G. Golub, C. van Loan, *Matrix Computations* (The Johns Hopkins University Press, Baltimore, MD, 1996)
13. S. Pillai, C. Kwon, Forward/backward spatial smoothing techniques for coherent signal identification. IEEE Trans. Acoust. Speech Signal Process. **37**(1), 8–15 (1989)
14. P. Stoica, A. Nehorai, MUSIC, maximum likelihood, and the cramér-Rao bound. IEEE Trans. Acoust. Speech Signal Process. **37**(5), 720–741 (1989)
15. Y. Abramovich, B. Johnson, X. Mestre, Performance breakdown in MUSIC, G-MUSIC and maximum likelihood estimation, in *Proc. of the 32nd IEEE Int. Conf. on Acoustics, Speech and Sig. Proc. (ICASSP)*, Honolulu, USA, 2007
16. I. Ziskind, M. Wax, Maximum likelihood localization of multiple sources by alternating projection. IEEE Trans. Acoust. Speech Signal Process. **36**(10), 1553–1560 (1988)
17. J. Li, D. Zheng, P. Stoica, Angle and waveform estimation via RELAX. IEEE Trans. Aerosp. Electron. Syst. **33**(3), 1077–1087 (1997)
18. B. Ottersten, M. Viberg, P. Stoica, A. Nehorai, Exact and large sample ML techniques for parameter estimation and detection in array processing, in *Radar Array Processing* (Springer, Berin, 1993)
19. P. Heidenreich, *Antenna Array Processing: Autocalibration and Fast High-Resolution Methods for Automotive Radar,* Ph.D. thesis, Technische Universität Darmstadt, 2012

20. A. Lee, Centrohermitian and skew-centrohermitian matrices. Linear Algebra Appl. **29**, 205–210 (1980)
21. M. Pesavento, A. Gershman, M. Haardt, Unitary root-MUSIC with a real-valued eigendecomposition: a theoretical and experimental performance study. IEEE Trans. Signal Process. **49**(5), 1306–1314 (2000)
22. P. Heidenreich, A. Zoubir, Computationally simple DOA estimation of two resolved targets with a single snapshot, in *Proc. of the 37th IEEE Int. Conf. on Acoustics, Speech and Sig. Proc. (ICASSP)*, Kyoto, Japan, 2012